



Full length article



QH-POCC: Taming tiling entropy in thermal expansion calculations of disordered materials

Marco Esters^{a,b,1}, Andriy Smolyanyuk^{c,b,1}, Corey Oses^{a,b}, David Hicks^b, Simon Divilov^{a,b}, Hagen Eckert^{a,b}, Xiomara Campilongo^b, Cormac Toher^{d,b}, Stefano Curtarolo^{a,b,*}

^a Department of Mechanical Engineering and Materials Science, Duke University, Durham, NC 27708, USA

^b Center for Autonomous Materials Design, Duke University, Durham, NC 27708, USA

^c Institute of Solid State Physics, Technische Universität Wien, A-1040 Wien, Austria

^d Department of Materials Science and Engineering and Department of Chemistry and Biochemistry, University of Texas at Dallas, Richardson, TX 75080, USA

ARTICLE INFO

Dataset link: [AFLOW.org](https://aflo.wflow.org)

Keywords:

Thermal expansion calculation
Disordered systems
Solid solutions
High entropy alloys
High entropy ceramics

ABSTRACT

Disordered materials are attracting considerable attention because of their enhanced properties compared to their ordered analogs, making them particularly suitable for high-temperature applications. The feasibility of incorporating these materials into new devices depends on a variety of thermophysical properties. Among them, thermal expansion is critical to device stability, especially in multi-component systems. Its calculation, however, is quite challenging for materials with substitutional disorder, hindering computational screenings. In this work, we introduce QH-POCC to leverage the local tile-expansion of disorder. This method provides an effective partial partition function to calculate thermomechanical properties of substitutionally disordered compounds in the quasi-harmonic approximation. Two systems, AuCu₃ and CdMg₃, the latter a candidate for long-period superstructures at low temperature, are used to validate the methodology by comparing the calculated values of the coefficient of thermal expansion and isobaric heat capacity with experiment, demonstrating that QH-POCC is a promising approach to study thermomechanical properties of disordered systems.

1. Introduction

Multi-component alloys (MCAs) and ceramics (MCCs) are novel classes of materials offering enhanced properties such as ultra-high hardness [1,2], low thermal conductivity [3], and good corrosion and wear resistance [4–6]. The combination of these properties makes them suitable for applications in thermal barrier coatings [7], thermoelectrics [8], ultra-high temperature structural applications [9], and diffusion barriers for microelectronics [10]. In these types of applications, a material is often part of a multi-component system. It is thus not only critical for the material to have optimized properties, but it must also be compatible with the remaining parts of the device at operating conditions [11]. For example, combining components with incompatible coefficients of thermal expansion (CTEs) would compromise the integrity of the product at higher temperatures.

While measuring CTEs has become an increasingly integral part of experimental research of MCAs and MCCs [12–15], the substitutional disorder presents a formidable challenge for computational investigations of these materials, resulting in only few computed CTE values

with scarce experimental validation [16,17]. To date, calculations of thermal expansion in systems with substitutional disorder have employed the Coherent Potential Approximation (CPA) [18,19], Special Quasirandom Structures (SQS) [20], or the cluster expansion (CE) method [21,22]. The CPA allows for modeling alloys of any stoichiometry using relatively small unit cells. However, it cannot reliably calculate atomic forces [23] and is thus unable to employ conventional lattice dynamics methods. SQS models disordered systems at a fixed composition by finding the most random (infinite temperature) representation of the structure. As a consequence, it neglects finite-temperature short-range ordering effects. CE calculates thermodynamic properties through a series expansion of the free energy using a set of ordered structures. While the obtained free energy is exact, the combinatorial explosion of the number of cluster expansion parameters makes the study of complex MCAs and MCCs impractical.

The Partial OCCupation (POCC) method was developed to include finite-temperature effects while alleviating the computational cost of CE [24], thus allowing practical studies of multi-component systems.

* Corresponding author at: Center for Autonomous Materials Design, Duke University, Durham, NC 27708, USA.

E-mail address: stefano@duke.edu (S. Curtarolo).

¹ These two authors contributed equally.

POCC models the disordered material through a series of small *tiles* – ordered representative supercells with the same stoichiometry as the parent structure – which are also capable of calculating vibrational properties [25]. This particular expansion allows POCC to factorize the *tiling entropy* associated with the latent heat of a first order phase transition (from chemical order and microstructural disorder to chemical disorder and no microstructures), and to generate a partial partition function out of the global one. The approach, taken at finite temperatures with the quasi-harmonic approximation (QHA), enables the calculation of thermomechanical properties. The extended method, called QH-POCC, is tested on AuCu₃ and CdMg₃ for the ordered and disordered fields. Both thermal expansion and isobaric heat capacity are in good agreement with experiments, demonstrating the potential of QH-POCC to accurately model thermomechanical properties in the QHA at a reasonable computational cost. We chose the latter compound for its capabilities in forming long-period superstructures at low temperature [26–28], so that the effect of the diverging characteristic lengths of the ground-state can be qualitatively compared against the finite size of the POCC tiles expansion.

2. Computational methods

Thermal Expansion of Disordered Systems. The volumetric CTE β is defined as the logarithmic derivative of the temperature-dependent equilibrium volume:

$$\beta = \frac{d \log(V_{\text{eq}}(T))}{dT} = \frac{1}{V_{\text{eq}}(T)} \frac{dV_{\text{eq}}(T)}{dT}, \quad (1)$$

where $V_{\text{eq}}(T)$ is the equilibrium volume at temperature T , i.e., the volume V for which the temperature- and volume-dependent free energy F is at a minimum:

$$\frac{\partial F(V, T)}{\partial V} = 0. \quad (2)$$

$F(V, T)$ consists of the following contributions when neglecting anharmonic effects:

$$F(V, T) = E_0(V) + F_{\text{elec}}(V, T) + F_{\text{vib}}(V, T). \quad (3)$$

E_0 is the energy of the structure at 0 K. F_{elec} is the electronic contribution to the free energy and can be calculated as:

$$F_{\text{elec}}(V, T) = U_{\text{elec}} - TS_{\text{elec}}, \quad (4)$$

$$U_{\text{elec}}(V, T) = \int_0^{\infty} f_{\text{FD}} g_{\text{e}}(\epsilon, V) \epsilon d\epsilon - \int_0^{E_{\text{F}}} g_{\text{e}}(\epsilon, V) \epsilon d\epsilon, \quad (5)$$

$$S_{\text{elec}}(T) = -k_{\text{B}} \int_0^{\infty} g_{\text{e}}(\epsilon, V) s_{\text{T}}(\epsilon) d\epsilon. \quad (6)$$

Here, $g_{\text{e}}(\epsilon, V)$ is the electronic density of states (DOS), $f_{\text{FD}} = f_{\text{FD}}(\epsilon, T)$ is the Fermi–Dirac distribution, E_{F} is the Fermi energy, and $s_{\text{T}}(\epsilon) = f_{\text{FD}} \log(f_{\text{FD}}) + (1 - f_{\text{FD}}) \log(1 - f_{\text{FD}})$ is the electronic entropy of ϵ .

The last contribution, F_{vib} , is the vibrational free energy. It can be calculated via the phonon DOS, $g_{\text{ph}}(\omega(V))$, as:

$$F_{\text{vib}}(V, T) = k_{\text{B}} T \int_0^{\infty} \log \left(2 \sinh \frac{\hbar \omega(V)}{2k_{\text{B}} T} \right) g_{\text{ph}}(\omega(V)) d\omega, \quad (7)$$

where ω is the phonon frequency and \hbar is the reduced Planck constant.

In the QHA, $V_{\text{eq}}(T)$ is obtained by calculating $F(V, T)$ over a set of volumes and fitting the volume-dependent free energy to an equation of state (EOS) for each temperature. Calculating the volume-dependency of F is thus the central problem for the calculation of thermomechanical properties at finite temperatures.

Computational modeling of MCAs and MCCs – and therefore accurate calculation of free energies – is challenging due to the substitutional disorder in these compounds. AFLOW-POCC describes disordered materials through an ensemble of small Hermite-normal-form (HNF) ordered representatives [29–31], also called *tiles*. This method reproduces the correct composition, symmetry, and properties that depend

on the radial distribution function of the system but needs to be integrated over all possible *tiling configurations* if the global partition function Z_{global} and free energy F_{global} are needed. For an NVT ensemble, Z_{global} can be calculated as:

$$Z_{\text{global}}(V, T) \equiv \sum_{\substack{i\text{-tiles} \\ \text{tiling}\{V_i\}=V}} g_i \exp \left(-\frac{F_i(V_i, T)}{k_{\text{B}} T} \right), \quad (8)$$

where k_{B} is the Boltzmann constant and V_i is the volume of the i th tile. The sum is constrained by the organization of the tiles covering the whole normalized volume $\sum \{V_i\} / N = V$ with the global number of tiles N . $Z_{\text{global}}(V, T)$ can be used to obtain F_{global} through:

$$F_{\text{global}}(V, T) \equiv -k_{\text{B}} T \log Z_{\text{global}}(V, T). \quad (9)$$

The calculation of $Z_{\text{global}}(V, T)$ is highly non-trivial. The number of possible configurations Ω_{tiling} – having the correct volume where all the pieces fit together – increases with the cut off of the maximum POCC tile-size. Thermodynamically, this number also leads to the tiling entropy $S_{\text{tiling}} \equiv k_{\text{B}} \log \Omega_{\text{tiling}}$. The properties describing the “organization”, $\{\Omega_{\text{tiling}}, S_{\text{tiling}}\}$, can be calculated combinatorially or through Monte Carlo modeling like in percolation or self-avoiding random-walks theories, but incurs great computational cost. Here, these quantities can be neglected because of the following considerations:

i. Ω_{tiling} varies slowly unless near a first-order phase transition. The number of possible configurations depends on the identity and distribution of the individual tiles. Therefore, Ω_{tiling} is nearly constant below and above the transition temperature, albeit not the same in general. At the phase transition, on the other hand, the Boltzmann population vector suddenly rotates in the probability hyperspace (see Fig. 2e in Ref. [32]), leading to completely different tiling-distribution identities and thus a different Ω_{tiling} . Similar considerations hold for the tiling entropy: $S_{\text{tiling}}(T)$ is a slowly varying function of T unless a phase transition is crossed.

ii. Derivatives $\partial[\cdot]/\partial T$ operating on functionals containing $S_{\text{tiling}}(T)$ may ignore tiling contributions. As long as $\partial[\cdot]/\partial T$ is not operated at the phase transition (or nearby, as precursors start appearing [32]), $S_{\text{tiling}}(T)$ can be neglected with great computational savings. Temperature-derivative properties, such as specific heat and thermal expansion, can be estimated below and above the transition temperature without direct knowledge of the organization of the tiles.

iii. Once the tiling organization is settled, phase stability requires minimization of free energies. This, in turn, requires minimization with respect the total tiling organization along the aforementioned volume constraints, $\sum \{V_i\} / N = V$ (Lie derivative). In general, $\min[\sum \{\cdot\}] \neq \sum \min[\{\cdot\}]$ – yet, the POCC model allows to solve this conundrum: in canonical POCC-tiles, both species concentration and superlattice are conserved. Only atoms are swapped generating symmetrically inequivalent decorations [24]. As such, the volumes V_i and minimum energy E_i (or H_i in an applied stress field) for each i -tile will be quite close, $V_i \sim V$, so that the global EOS can be summarized as:

$$\begin{aligned} \min[\text{EOS}\{V_i\}] &\equiv \min \left[\sum_i \text{EOS}_i(V_i) \right] \approx \\ &\approx \sum_i \min[\text{EOS}_i(V_i)] \approx \sum_i \text{EOS}_i(V). \end{aligned} \quad (10)$$

Eq. (10) coupled with Eqs. (8) and (9) allow the definition of a partial partition function $Z_{\text{POCC}}(V, T)$ and free energy $F_{\text{POCC}}(V, T)$:

$$Z_{\text{POCC}}(V, T) \equiv \sum_{i\text{-tiles}} g_i \exp \left(-\frac{F_i(V, T)}{k_{\text{B}} T} \right), \quad (11)$$

$$F_{\text{POCC}}(V, T) \equiv -k_{\text{B}} T \log Z_{\text{POCC}}(V, T). \quad (12)$$

Even though Z_{POCC} and F_{POCC} neglect tiling entropy, they are capable of reproducing T -derivative properties outside regions of phase transition, without the cumbersome calculation of the global partition

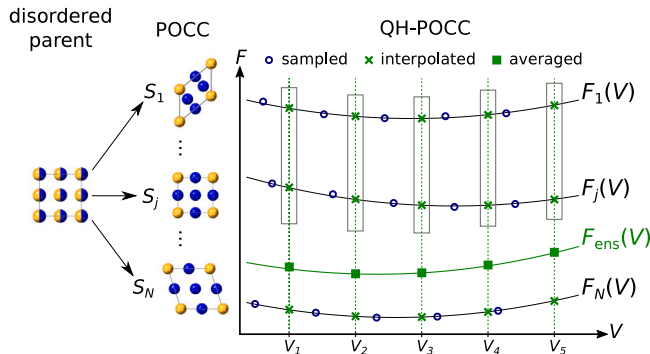


Fig. 1. Illustration of the QH-POCC workflow. The free energies of the AFLOW-POCC tiles $\{S_i\}$ are sampled for various volumes near the equilibrium. The free energies are interpolated and then ensemble-averaged to resolve the free energy of the disordered system, from which thermomechanical properties can be derived.

function. Eq. (12) can then be used to construct the EOS of the disordered material, leading to the global coefficient of thermal expansion via Eq. (1). This scheme is illustrated in Fig. 1.

From the EOS-fitted curve, other thermomechanical properties can be derived. The isobaric (C_p) and isochoric (C_v) heat capacities can be calculated as:

$$C_p = -T \left(\frac{\partial^2 F_{\text{POCC}}(V, T)}{\partial T^2} \right)_p = -T \frac{\partial^2 F_{\text{POCC}}(V_{\text{eq}}, T)}{\partial T^2}, \quad (13)$$

$$C_v = C_p - V_{\text{eq}} B \beta^2 T, \quad (14)$$

where B is the bulk modulus:

$$B = V \frac{\partial^2 F_{\text{POCC}}(V, T)}{\partial V^2}. \quad (15)$$

These quantities can be used to determine the effective Grüneisen parameter $\bar{\gamma}$:

$$\bar{\gamma} = \frac{V_{\text{eq}} B \beta}{C_v}. \quad (16)$$

Calculations' details. AFLOW [40] leverages the Vienna *ab initio* simulation package (VASP) with all calculation parameters following the AFLOW standard [41]. Exchange and correlation were treated with the projector augmented wave (PAW) method [42] in either the local density approximation (LDA) [43] or generalized gradient approximation (GGA) proposed by Perdew, Burke, and Ernzerhof (PBE) [44]. The cutoff energies are chosen to be 1.4 times the recommended maximum cutoffs (ENMAX) of all pseudopotentials as set by VASP.

Disordered compounds were modeled using the AFLOW-POCC module with a supercell size of 4, resulting in 7 and 29 unique tiles, respectively. Phonon calculations were performed using the AFLOW-APL module [25]. Supercell sizes and k -point mesh dimensions were selected such that free energies were converged to within 1 meV/atom for representative tiles of the disordered materials. For ordered representatives of CdMg_3 , the supercells used to calculate the phonon properties were constructed to have at least 64 atoms, while for the ordered representatives of AuCu_3 , the sizes were chosen as specified in Table 1. Forces within these supercells were calculated with a k -points mesh having at least 6900 and 3000 k -points per reciprocal atom (KPPRA) for AuCu_3 and CdMg_3 , respectively [41].

For the EOS fit, vibrational properties were calculated at various compressed and expanded volumes, typically spanning -12% to 12% of the equilibrium volume at a 6% increment. For AuCu_3 , adjustments needed to be made to accommodate for the presence of imaginary frequencies (see Table 1). Ordered representative #3 of AuCu_3 has unstable modes with the LDA functional at 3% volume compression, but these modes were easily omitted in the calculation of the thermo-mechanical properties because their contributions to the phonon DOS

Table 1

Parameters for the QHA calculations of the ordered representatives of AuCu_3 . The volume range is given in percent and in the format *initial:final:increment*. Negative values denote compression, positive values expansion of the cell. rhl: rhombohedral, orc: orthorhombic, mcl: base-centered monoclinic, tet: tetragonal, bct: body-centered tetragonal, orcc: base-centered orthorhombic, cub: simple cubic.

POCC structure	Supercell	Lattice type	Volume change (%)
1	$2 \times 2 \times 2$	rhl	-12:12:6
2	$2 \times 2 \times 1$	orc	-12:12:6
3	$2 \times 2 \times 1$	mcl	-3:12:6
4	$3 \times 3 \times 2$	tet	-12:12:6
5	$2 \times 2 \times 2$	bct	-12:12:6
6	$2 \times 2 \times 4$	orcc	-6:12:6
7	$2 \times 2 \times 2$	cub	-12:12:6

were negligible. Ordered representative #4 of AuCu_3 was found to be dynamically unstable and was discarded entirely from the ensemble of structures. The calculated free energies were fitted using the Stabilized Jellium EOS [45,46]:

$$F(V) = \sum_{i=0}^3 f_i V^{-\frac{1}{3}i}. \quad (17)$$

The parameters f_i were determined using a polynomial fit.

3. Results and discussion

Two disordered alloys are used to validate the QH-POCC method: AuCu_3 and CdMg_3 . These compounds were chosen due to their simple crystal structures and readily available experimental data. AuCu_3 is ordered at low temperatures and crystallizes in the $L1_2$ structure (AFLOW prototype [AB3_cp4_221_a_c](#) [47–49]). Above 450 K, it becomes partially disordered and then fully disordered above 663 K, where it adopts a face-centered cubic crystal structure (AFLOW prototype [A_cf4_225_a](#)) [33,50]. CdMg_3 transitions from its ordered $D0_{19}$ phase (AFLOW prototype [A3B_hP8_194_h_c](#)) to a hexagonal close-packed disordered structure at 423 K [35,51].

Fig. 2 shows the calculated thermomechanical properties for these materials in their ordered and disordered phases using the Local Density Approximation (LDA) and the Perdew–Burke–Ernzerhof (PBE) functional. For both ordered and disordered AuCu_3 , β increases with increasing temperature until they plateau above 200 K (Fig. 2a). The CTE of the disordered structure is larger than of the ordered phase for all temperatures, which is consistent with experiment. PBE overestimates experimental β values for both states. The disordered phase even appears to diverge at higher temperatures, which is expected for QHA, as anharmonic contributions become increasingly dominant. LDA shows excellent agreement with experimental values, suggesting that the choice of the functional is the reason for the bad agreement for PBE.

The CTE of CdMg_3 is shown in Fig. 2b. The curves of the ordered phases show similar behavior as those for AuCu_3 , except for β for LDA, which converges towards the value of the disordered phase. Good experimental values for the ordered phase are unavailable in literature, but extrapolating from the tail found in the experimental values, it is anticipated to see good agreement. Above the experimental order–disorder transition temperature, the disordered phase shows good agreement for PBE whereas LDA underestimates β . This shows that the functional choice is critical when calculating thermal expansion of these materials. QH-POCC also shows a striking difference in the disordered phase compared to AuCu_3 : β of disordered CdMg_3 exhibits a peak at 50 K and 70 K for PBE and LDA, respectively.

The isobaric heat capacities shown in Fig. 2c for AuCu_3 and in Fig. 2d for CdMg_3 are less sensitive to the chosen functional. The agreement with experimental values for the ordered structures is excellent for both functionals. C_p for the disordered phases are underestimated, but still in good agreement with experiments. A peak can be observed

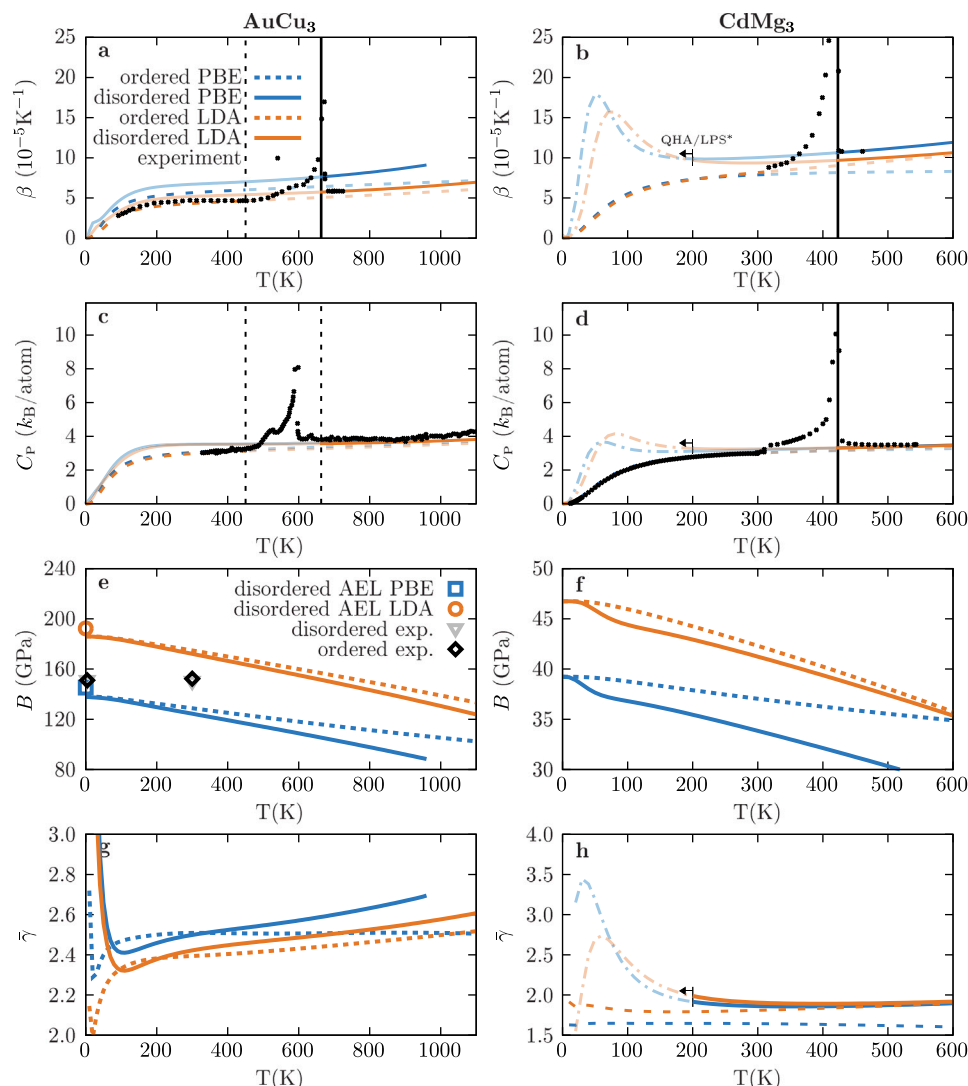


Fig. 2. Thermomechanical properties of Cu_3Au and CdMg_3 from QH-POCC. a, b Thermal expansion coefficient β , c, d isobaric heat capacity C_p , e, f bulk modulus B , and g, h effective Grüneisen parameter $\bar{\gamma}$ of AuCu_3 (left) and CdMg_3 (right). The dashed vertical lines for AuCu_3 represent the transition temperatures to the partially and the fully disordered states, respectively. The dashed vertical lines for CdMg_3 denote the transition temperature to the disordered structure. Experimental values are taken from Refs. [33–38]. Note “QHA/LPS*”. For CdMg_3 , the unphysical peaks of thermal expansion, heat capacity and Grüneisen parameter, suggest the formation of long-period superstructures (LPS), modulations of the hexagonal ordered structure D0_{19} taken as reference for the POCC expansion. The finite-size cutoff of the tiles cannot represent the divergence of the characteristic lengths of the long-period superstructures. Thus, the constrained LTVC population vector [32] will rotate and promote modifications of D0_{19} containing antiphase boundaries [39] (with increasing volume) without reaching full LPS description.

in QH-POCC for both LDA and PBE in disordered CdMg_3 , with the peak for LDA being at a higher temperature.

For the bulk modulus, experimental data is only available for AuCu_3 [38]. As Fig. 2e shows, PBE underestimates B whereas LDA strongly overestimates it. B is very sensitive to the chosen functional since it depends on the volume of the unit cell. This is not a shortcoming of QH-POCC, but of QHA, as this behavior was also found for simple ordered materials such as MgO and CaO [52]. To further substantiate that QH-POCC is consistent with other methods, B was calculated at 0 K using the AFLOW Automatic Elastic Library (AEL) [53] — Fig. 2e demonstrates that AEL and QH-POCC are consistent with each other. The values for the disordered phase is smaller than for the ordered phase at all temperatures, which is consistent with experiments. However, B drops much faster with temperature than experiments suggest, which has also been observed in ordered materials [52].

As for AuCu_3 , CdMg_3 has a smaller bulk modulus in the disordered than in the ordered state, with LDA resulting in larger moduli than PBE. The temperature dependence of disordered CdMg_3 differs from AuCu_3 by showing an inflection, the end point of which coincides with the temperature of the peak in β and C_p for both functionals.

Finally, Figs. 2g and h show the effective Grüneisen parameters for both materials. In general, $\bar{\gamma}$ is larger for the disordered material than the ordered material, particularly at higher temperatures. An exception is LDA and CdMg_3 , where $\bar{\gamma}$ for the ordered phase approaches the disordered phase due to the divergence of β at higher temperatures. Higher values of $\bar{\gamma}$ correlate with lower thermal conductivity, which is expected for materials with substitutional disorder [3]. The divergences found at low temperatures are the result of the calculation method: as Eq. (16) shows, $\bar{\gamma}$ depends on the quotient of β and C_v , both of which are very small at low temperatures, causing numerical instabilities. This relationship also causes the peak for CdMg_3 as β peaks stronger than C_p .

In experiments, peaks in thermal expansion and isobaric heat capacity typically indicate phase transitions. Here, peaks are not found in QHA for ordered phases and in disordered CdMg_3 regions. From the solid solution and upon reducing temperature, CdMg_3 transitions from a disordered hexagonal close-packed structure to the ordered D0_{19} [26,51]. With further temperature reduction, D0_{19} often develops antiphase boundaries and complex stacking faults [39], associated with

forming long-period superstructures (LPS). Notably, several Cd and Mg binary alloys show similar features [26–28]. The divergence of the characteristic length scale in the LPS cannot be reproduced by the tiles having a finite size, making the POCC expansion incomplete. Therefore, the constrained LTVC population vector [32] will rotate and promote modifications of $D0_{19}$ containing antiphase boundaries and stacking faults having increased volume without ever reaching full LPS description. While such computational limitation is expected to appear at low temperatures and in all systems having ordered ground-states with characteristic length scales too large for the POCC-tiles expansion, our algorithm has been devised to study disordered systems at high temperatures where only short-range needs to be described [11,54]. As such, the limitation does not pose any concern.

Experiments suggest that a peak should appear in β and C_p for $AuCu_3$ as well, but none are observable in Figs. 2a and c. The reason for this discrepancy could be the sample size of the canonical ensemble: POCC creates only 7 ordered representatives for $AuCu_3$, but 29 for $CdMg_3$. To test this hypothesis, the size of the HNF matrix was increased to 8, which produced 49 ordered representatives. As Figs. 3a and b show, increasing the maximum POCC tile size results in a peak in both thermal expansion and heat capacity, confirming that small sampling suppressed the appearance of the phase transition. However, no inflection point can be observed in the bulk modulus as was observed in $CdMg_3$ (see Fig. 3c). This is not surprising because the values for the ordered and disordered phase are similar at low temperatures in both QH-POCC and experiments, making any inflection imperceptible. Finally, the effective Grüneisen parameter, shown in Fig. 3d, shows a deep dip at lower temperatures when the supercell size is increased due to the larger peak height in C_p , which is in the denominator of $\bar{\gamma}$.

As with $CdMg_3$, the calculated transition temperature of $AuCu_3$ is far below the experimental value. While transitioning from an ordered to a disordered phase, both materials are in a partially ordered state spanning at least 100 K. The requirement of POCC that the stoichiometry of the tiles correspond to the disordered structure parametrizes this transition region as a line. To improve the accuracy of the transition temperature, a more complete picture of the tile distribution is needed so that the variation of S_{tiling} can be captured. This could be achieved, for example, by including structures with compositions different from the parent structure. A similar approach is employed in the Lederer-Toher-Vecchio-Curtarolo (LTVC) method, which can accurately predict the transition temperature, but requires more input data [32].

Outside the transition region, however, all properties are well converged with respect to the POCC supercell size. So, while Ω_{tiling} and S_{tiling} may change with increased maximum tile size, their temperature derivatives do not. The smallest supercell is thus sufficient to calculate thermophysical properties of the disordered material.

4. Conclusions

This work introduces a new framework, QH-POCC, to perform finite temperature calculations of thermophysical properties of systems with substitutional disorder. The method uses the Partial Occupation algorithm and the quasi-harmonic approximation (QHA) to calculate finite-temperature free energies using a canonical ensemble. This ensemble is then used to determine properties accessible via the QHA. Two systems, $AuCu_3$ and $CdMg_3$, were used to validate the approach by comparing calculated values of thermal expansion and isobaric heat capacity with experimental data. The results are in a good agreement with experiments, demonstrating that QH-POCC is a promising method to study finite-temperature vibrational properties. Due to the implicit incorporation of the configurational energy, QH-POCC is able to recover features that are inaccessible to methods that rely on only one supercell. Peaks in both thermal expansion and heat capacity indicate structural phase transitions. The combination of computational efficiency, capability to bypass the calculation of the tiling-entropy, and overall accuracy makes QH-POCC an excellent screening tool for thermomechanical properties of disordered materials in the quasi-harmonic approximation.

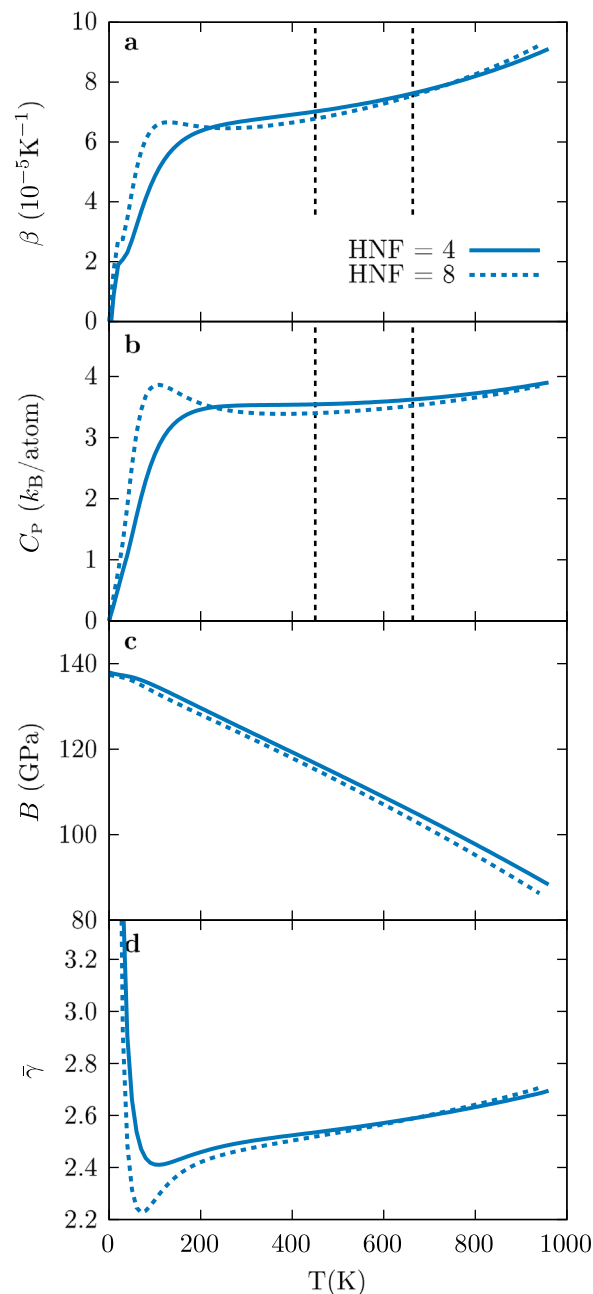


Fig. 3. Thermomechanical properties of Cu_3Au for larger POCC supercells. a Thermal expansion coefficient β , b isobaric heat capacity C_p , c bulk modulus B , and d effective Grüneisen parameter $\bar{\gamma}$ of $AuCu_3$ for POCC supercell sizes (HNF) 4 (solid lines) and 8 (dash-dotted lines). The dashed vertical lines represent the transition temperatures to the partially and the fully disordered state, respectively.

Software availability

The code is freely available as part of the AFLOW software suite [40]. All information to reproduce the data are documented in this article.

Declaration of competing interest

The authors declare that they have no known competing financial interests or personal relationships that could have appeared to influence the work reported in this paper.

Data availability

All structure data is freely available and accessible online through [AFLOW.org](https://aflo.org) [55] or programmatically via the REST- [56] and AFLUX Search-APIs [57].

Acknowledgments

The authors thank Mark Asta, Zi-Kui Liu, Axel van de Walle, and Adam Zettl for valuable discussions. Research sponsored by DOD-ONR (N00014-15-1-2863 , N00014-21-1-2515) and NSF (DMR-1921909, DGE-2022040).

References

- P. Sarker, T. Harrington, C. Toher, C. Oses, M. Samiee, J.-P. Maria, D.W. Brenner, K.S. Vecchio, S. Curtarolo, High-entropy high-hardness metal carbides discovered by entropy descriptors, *Nature Commun.* 9 (2018) 4980, <https://doi.org/10.1038/s41467-018-07160-7>.
- Y. Wang, T. Csanádi, H. Zhang, J. Dusza, M.J. Reece, R.-Z. Zhang, Enhanced hardness in high-entropy carbides through atomic randomness, *Adv. Theory Simul.* 3 (2020) 2000111, <https://doi.org/10.1002/adts.202000111>.
- J.L. Braun, C.M. Rost, M. Lim, A. Giri, D.H. Olson, G.N. Kotsonis, G. Stan, D.W. Brenner, J.-P. Maria, P.E. Hopkins, Charge-induced disorder controls the thermal conductivity of entropy-stabilized oxides, *Adv. Mater.* 30 (2018) 1805004, <https://doi.org/10.1002/adma.201805004>.
- M.-H. Tsai, J.-W. Yeh, High-entropy alloys: A critical review, *Mater. Res. Lett.* 2 (2014) 107–123, <https://doi.org/10.1080/21663831.2014.912690>.
- Y.F. Ye, Q. Wang, J. Lu, C.T. Liu, Y. Yang, High-entropy alloy: challenges and prospects, *Mater. Today* 19 (2016) 349–362, <https://doi.org/10.1016/j.mattod.2015.11.026>.
- C. Oses, C. Toher, S. Curtarolo, High-entropy ceramics, *Nat. Rev. Mater.* 5 (2020) 295–309, <https://doi.org/10.1038/s41578-019-0170-8>.
- L. Zhou, F. Li, J.-X. Liu, Q. Hu, W. Bao, Y. Wu, X. Cao, F. Xu, G.-J. Zhang, High-entropy thermal barrier coating of rare-earth zirconate: A case study on $(La_{0.2}Nd_{0.2}Sm_{0.2}Eu_{0.2}Gd_{0.2})_2Zr_2O_7$ prepared by atmospheric plasma spraying, *J. Eur. Ceram. Soc.* 40 (2020) 5731–5739, <https://doi.org/10.1016/j.jeurceramsoc.2020.07.061>.
- B. Jiang, Y. Yu, J. Cui, X. Liu, L. Xie, J. Liao, Q. Zhang, Y. Huang, S. Ning, B. Jia, B. Zhu, S. Bai, L. Chen, S.J. Pennycook, J. He, High-entropy-stabilized chalcogenides with high thermoelectric performance, *Science* 371 (2021) 830–834, <https://doi.org/10.1126/science.abe1292>.
- E. Wuchina, E. Opila, M. Opeka, W. Fahrenholtz, I. Talmay, UHTCs: Ultra-High Temperature Ceramic Materials for Extreme Environment Applications, *Electrochem. Soc. Interface* 16 (2007) 30–36.
- M.-H. Tsai, C.-W. Wang, C.-H. Lai, J.-W. Yeh, J.-Y. Gan, Thermally stable amorphous $(AlMoNbSiTaTiVZr)_{50}N_{50}$ nitride film as diffusion barrier in copper metallization, *Appl. Phys. Lett.* 92 (2008) 052109, <https://doi.org/10.1063/1.2841810>.
- G.S. Rohrer, M. Affatigato, M. Backhaus, R.K. Bordia, H.M. Chan, S. Curtarolo, A. Demkov, J.N. Eckstein, K.T. Faber, J.E. Garay, Y. Gogotsi, L. Huang, L.E. Jones, S.V. Kalinin, R.J. Lad, C.G. Levi, J. Levy, J.-P. Maria, L. Mattos Jr., A. Navrotsky, N. Orlovskaya, C. Pantano, J.F. Stebbins, T.S. Sudarshan, T. Tani, K.S. Weil, Challenges in ceramic science: A report from the workshop on Emerging Research Areas in ceramic science, *J. Am. Ceram. Soc.* 95 (2012) 3699–3712, <https://doi.org/10.1111/jace.12033>.
- G. Laplanche, P. Gadaud, C. Bärsch, K. Demtröder, C. Reinhart, J. Schreuer, E.P. George, Elastic moduli and thermal expansion coefficients of medium-entropy subsystems of the CrMnFeCoNi high-entropy alloy, *J. Alloys Compd.* 746 (2018) 244–255, <https://doi.org/10.1016/j.jallcom.2018.02.251>.
- J. Zhu, X. Meng, J. Xu, P. Zhang, Z. Lou, M.J. Reece, F. Gao, Ultra-low thermal conductivity and enhanced mechanical properties of high-entropy rare earth niobates (RE_3NbO_7 , RE=Dy, Y, Ho, Er, Yb), *J. Eur. Ceram. Soc.* 41 (2021) 1052–1057, <https://doi.org/10.1016/j.jeurceramsoc.2020.08.070>.
- J. Zhu, X. Meng, P. Zhang, Z. Li, J. Xu, M.J. Reece, F. Gao, Dual-phase rare-earth-zirconate high-entropy ceramics with glass-like thermal conductivity, *J. Eur. Ceram. Soc.* 41 (2021) 2861–2869, <https://doi.org/10.1016/j.jeurceramsoc.2020.11.047>.
- L. Chen, Y. Wang, M. Hu, L. Zhang, J. Wang, Z. Zhang, X. Liang, J. Guo, J. Feng, Achieved limit thermal conductivity and enhancements of mechanical properties in fluorite RE_3NbO_7 via entropy engineering, *Appl. Phys. Lett.* 118 (2021) 071905, <https://doi.org/10.1063/5.0037373>.
- D. Ma, B. Grabowski, F. Körmann, J. Neugebauer, D. Raabe, Ab initio thermodynamics of the CoCrFeMnNi high entropy alloy: Importance of entropy contributions beyond the configurational one, *Acta Mater.* 100 (2015) 90–97, <https://doi.org/10.1016/j.actamat.2015.08.050>.
- S. Huang, Á. Vida, W. Li, D. Molnár, S. Kyun Kwon, E. Holmström, B. Varga, L. Károly Varga, L. Vitos, Thermal expansion in FeCrCoNiGa high-entropy alloy from theory and experiment, *Appl. Phys. Lett.* 110 (2017) 241902, <https://doi.org/10.1063/1.4985724>.
- P. Soven, Coherent-potential model of substitutional disordered alloys, *Phys. Rev.* 156 (1967) 809–813, <https://doi.org/10.1103/PhysRev.156.809>.
- B.L. Gyorffy, Coherent-potential approximation for a nonoverlapping-muffin-tin-potential model of random substitutional alloys, *Phys. Rev. B* 5 (1972) 2382–2384, <https://doi.org/10.1103/PhysRevB.5.2382>.
- A. Zunger, S.-H. Wei, L.G. Ferreira, J.E. Bernard, Special quasirandom structures, *Phys. Rev. Lett.* 65 (1990) 353–356, <https://doi.org/10.1103/PhysRevLett.65.353>.
- J.M. Sanchez, F. Ducastelle, D. Gratias, Generalized cluster description of multicomponent systems, *Physica A* 128 (1984) 334–350.
- D. de Fontaine, Cluster approach to order-disorder transformations in alloys, in: H. Ehrenreich, D. Turnbull (Eds.), *Solid State Physics*, Vol. 47, Academic Press, New York, 1994, pp. 33–176, [https://doi.org/10.1016/S0081-1947\(08\)60639-6](https://doi.org/10.1016/S0081-1947(08)60639-6).
- L. Vitos, Computational quantum mechanics for materials engineers: The EMTO Method and Applications, in: *Engineering Materials and Processes*, Springer, London, 2007.
- K. Yang, C. Oses, S. Curtarolo, Modeling off-stoichiometry materials with a high-throughput *Ab-Initio* Approach, *Chem. Mater.* 28 (2016) 6484–6492, <https://doi.org/10.1021/acs.chemmater.6b01449>.
- M. Esters, C. Oses, D. Hicks, M.J. Mehl, M. Jahnátek, M.D. Hossain, J.-P. Maria, D.W. Brenner, C. Toher, S. Curtarolo, Settling the matter of the role of vibrations in the stability of high-entropy carbides, *Nature Commun.* 12 (2021) 5747, <https://doi.org/10.1038/s41467-021-25979-5>.
- T.B. Massalski, H. Okamoto, P.R. Subramanian, L. Kacprzak (Eds.), *Binary Alloy Phase Diagrams*, ASM International, Materials Park, Ohio, USA, 1990.
- S. Curtarolo, D. Morgan, G. Ceder, Accuracy of *ab initio* methods in predicting the crystal structures of metals: A review of 80 binary alloys, *CALPHAD* 29 (2005) 163–211, <https://doi.org/10.1016/j.calphad.2005.01.002>.
- R.H. Taylor, S. Curtarolo, G.L.W. Hart, Guiding the experimental discovery of magnesium alloys, *Phys. Rev. B* 84 (2011) 084101, <https://doi.org/10.1103/PhysRevB.84.084101>.
- G.L.W. Hart, R.W. Forcade, Algorithm for generating derivative structures, *Phys. Rev. B* 77 (2008) 224115, <https://doi.org/10.1103/PhysRevB.77.224115>.
- A. Santoro, A.D. Mighell, Properties of crystal lattices: the derivative lattices and their determination, *Acta Cryst. A* 28 (1972) 284–287, <https://doi.org/10.1107/S0567739472000737>.
- A. Santoro, A.D. Mighell, Coincidence-site lattices, *Acta Cryst. A* 29 (1973) 169–175, <https://doi.org/10.1107/S0567739473000434>.
- Y. Lederer, C. Toher, K.S. Vecchio, S. Curtarolo, The search for high entropy alloys: A high-throughput *ab-initio* approach, *Acta Mater.* 159 (2018) 364–383, <https://doi.org/10.1016/j.actamat.2018.07.042>.
- F.C. Nix, D. MacNair, A dilatometric study of the order-disorder transformation in Cu-Au Alloys, *Phys. Rev.* 60 (1941) 320–329, <https://doi.org/10.1103/PhysRev.60.320>.
- H. Hirabayashi, S. Nagasaki, H. Kōno, Calorimetric study of Cu_3Au at High Temperatures, *J. Appl. Phys.* 28 (1957) 1070–1071, <https://doi.org/10.1063/1.1722915>.
- V. Hovi, P. Paalassalo, Dilatometric investigation of the order-disorder transition in Mg₂Cd, *Acta Metall.* 12 (1964) 723–729, [https://doi.org/10.1016/0001-6160\(64\)90219-6](https://doi.org/10.1016/0001-6160(64)90219-6).
- L.W. Coffer, R.S. Craig, C.A. Krier, W.E. Wallace, Magnesium-Cadmium Alloys. VII., Low temperature heat capacities of MgCd₃ and Mg₃Cd and a Test of the Third Law of Thermodynamics for the MgCd₃, *J. Am. Chem. Soc.* 76 (1954) 241–244, <https://doi.org/10.1021/ja01630a062>.
- W.V. Johnston, K.F. Sterrett, R.S. Craig, W.E. Wallace, Magnesium-Cadmium Alloys. VIII., Heat capacities of Mg₂Cd and MgCd₃ between 20 and 290° The Standard Heats, Free Energies and Entropies of Formation and the Residual Entropies, *J. Am. Chem. Soc.* 79 (1957) 3633–3637, <https://doi.org/10.1021/ja01571a004>.
- P.A. Flinn, G.M. McManus, J.A. Rayne, Elastic constants of ordered and disordered Cu_3Au from 4.2 to 300°K, *J. Phys. Chem. Solids* 15 (1960) 189–195, [https://doi.org/10.1016/0022-3697\(60\)90242-0](https://doi.org/10.1016/0022-3697(60)90242-0).
- P. Ghosal, S. Lele, Theory of diffraction from DO_{19} ordered c.p.h structures containing complex stacking faults on basal planes, *Acta Crystallogr. Sect. A* 59 (2003) 153–162, <https://doi.org/10.1107/S0108767302022316>.
- C. Oses, M. Esters, D. Hicks, S. Divilov, H. Eckert, R. Friedrich, M.J. Mehl, A. Smolyanyuk, X. Campilongo, A. van de Walle, J. Schroers, A.G. Kusne, I. Takeuchi, E. Zurek, M. Buongiorno Nardelli, M. Fornari, Y. Lederer, O. Levy, C. Toher, S. Curtarolo, aflow++: A C++ framework for autonomous materials design, *Comput. Mater. Sci.* 217 (2023) 111889, <https://doi.org/10.1016/j.commatsci.2022.111889>.
- C.E. Calderon, J.J. Plata, C. Toher, C. Oses, O. Levy, M. Fornari, A. Natan, M.J. Mehl, G.L.W. Hart, M. Buongiorno Nardelli, S. Curtarolo, The AFLOW standard for high-throughput materials science calculations, *Comput. Mater. Sci.* 108 (Part A) (2015) 233–238, <https://doi.org/10.1016/j.commatsci.2015.07.019>.

- [42] P.E. Blöchl, Projector augmented-wave method, *Phys. Rev. B* 50 (1994) 17953–17979, <http://dx.doi.org/10.1103/PhysRevB.50.17953>.
- [43] D.M. Ceperley, B.J. Alder, Ground state of the electron gas by a stochastic method, *Phys. Rev. Lett.* 45 (1980) 566–569, <http://dx.doi.org/10.1103/PhysRevLett.45.566>.
- [44] J.P. Perdew, K. Burke, M. Ernzerhof, Generalized gradient approximation made simple, *Phys. Rev. Lett.* 77 (1996) 3865–3868, <http://dx.doi.org/10.1103/PhysRevLett.77.3865>.
- [45] D.M. Teter, G.V. Gibbs, M.B. Boisen, D.C. Allan, M.P. Teter, First-principles study of several hypothetical silica framework structures, *Phys. Rev. B* 52 (1995) 8064–8073, <http://dx.doi.org/10.1103/PhysRevB.52.8064>.
- [46] A.B. Alchagirov, J.P. Perdew, J.C. Boettger, R.C. Albers, C. Fiolhais, Energy and pressure versus volume: Equations of state motivated by the stabilized jellium model, *Phys. Rev. B* 63 (2001) 224115, <http://dx.doi.org/10.1103/PhysRevB.63.224115>.
- [47] M.J. Mehl, D. Hicks, C. Toher, O. Levy, R.M. Hanson, G.L.W. Hart, S. Curtarolo, The AFLOW Library of Crystallographic Prototypes: Part 1, *Comput. Mater. Sci.* 136 (2017) S1–S828, <http://dx.doi.org/10.1016/j.commatsci.2017.01.017>.
- [48] D. Hicks, M.J. Mehl, E. Gossett, C. Toher, O. Levy, R.M. Hanson, G.L.W. Hart, S. Curtarolo, The AFLOW Library of Crystallographic Prototypes: Part 2, *Comput. Mater. Sci.* 161 (2019) S1–S1011, <http://dx.doi.org/10.1016/j.commatsci.2018.10.043>.
- [49] D. Hicks, M.J. Mehl, M. Esters, C. Oses, O. Levy, G.L.W. Hart, C. Toher, S. Curtarolo, The AFLOW Library of Crystallographic Prototypes: Part 3, *Comput. Mater. Sci.* 199 (2021) 110450, <http://dx.doi.org/10.1016/j.commatsci.2021.110450>.
- [50] D.T. Keating, B.E. Warren, Long-range order in beta-brass and Cu₃Au, *J. Appl. Phys.* 22 (1951) 286–290, <http://dx.doi.org/10.1063/1.1699944>.
- [51] M.D. Asta, R.P. McCormack, D. de Fontaine, Theoretical study of alloy phase stability in the Cd-Mg system, *Phys. Rev. B* 48 (1993) 748–766, <http://dx.doi.org/10.1103/PhysRevB.48.748>.
- [52] A. Erba, M. Shahrokhi, R. Moradian, R. Dovesi, On how differently the quasi-harmonic approximation works for two isostructural crystals: Thermal properties of periclase and lime, *J. Chem. Phys.* 142 (2015) 044114, <http://dx.doi.org/10.1063/1.4906422>.
- [53] C. Toher, C. Oses, J.J. Plata, D. Hicks, F. Rose, O. Levy, M. de Jong, M. Asta, M. Fornari, M. Buongiorno Nardelli, S. Curtarolo, Combining the AFLOW GIBBS and elastic libraries to efficiently and robustly screen thermomechanical properties of solids, *Phys. Rev. Mater.* 1 (2017) 015401, <http://dx.doi.org/10.1103/PhysRevMaterials.1.015401>.
- [54] A. Calzolari, C. Oses, C. Toher, M. Esters, X. Campilongo, S.P. Stepanoff, D.E. Wolfe, S. Curtarolo, Plasmonic high-entropy carbides, *Nature Commun.* 13 (2022) 5993, <http://dx.doi.org/10.1038/s41467-022-33497-1>.
- [55] M. Esters, C. Oses, S. Divilov, H. Eckert, R. Friedrich, D. Hicks, M.J. Mehl, F. Rose, A. Smolyanyuk, A. Calzolari, X. Campilongo, C. Toher, S. Curtarolo, aflow.org: A web ecosystem of databases, software and tools, *Comput. Mater. Sci.* 216 (2023) 111808, <http://dx.doi.org/10.1016/j.commatsci.2022.111808>.
- [56] R.H. Taylor, F. Rose, C. Toher, O. Levy, K. Yang, M. Buongiorno Nardelli, S. Curtarolo, A RESTful API for exchanging materials data in the AFLOWLIB.org consortium, *Comput. Mater. Sci.* 93 (2014) 178–192, <http://dx.doi.org/10.1016/j.commatsci.2014.05.014>.
- [57] F. Rose, C. Toher, E. Gossett, C. Oses, M. Buongiorno Nardelli, M. Fornari, S. Curtarolo, AFLUX: The LUX materials search API for the AFLOW data repositories, *Comput. Mater. Sci.* 137 (2017) 362–370, <http://dx.doi.org/10.1016/j.commatsci.2017.04.036>.